Biochimica et Biophysica Acta 1837 (2014) 366–374

Contents lists available at ScienceDirect

Biochimica et Biophysica Acta

journal homepage: www.elsevier.com/locate/bbabio

Structural and kinetic properties of *Rhodobacter sphaeroides* photosynthetic reaction centers containing exclusively Zn-coordinated bacteriochlorophyll as bacteriochlorin cofactors

Rafael G. Saer [a], Jie Pan [b], Amelia Hardjasa [a], Su Lin [b], Federico Rosell [c], A. Grant Mauk [c], Neal W. Woodbury [b], Michael E.P. Murphy [a], J. Thomas Beatty [a,*]

[a] Department of Microbiology and Immunology, The University of British Columbia, 2350 Health Sciences Mall, Vancouver, BC V6T 1Z3, Canada
[b] Department of Chemistry and Biochemistry and the Biodesign Institute, Arizona State University, Tempe, AZ 85287-1604, USA
[c] Department of Biochemistry and Molecular Biology and Centre for Blood Research, The University of British Columbia, 2350 Health Sciences Mall, Vancouver, BC V6T 1Z3, Canada

ARTICLE INFO

Article history:
Received 16 October 2013
Received in revised form 21 November 2013
Accepted 26 November 2013
Available online 5 December 2013

Keywords:
Bacteriochlorophyll
Reaction center
Bacteriopheophytin
Electron transfer
Rhodobacter sphaeroides
Spectroscopy

ABSTRACT

The Zn-BChl-containing reaction center (RC) produced in a *bchD* (magnesium chelatase) mutant of *Rhodobacter sphaeroides* assembles with six Zn-bacteriochlorophylls (Zn-BChls) in place of four Mg-containing bacteriochlorophylls (BChls) and two bacteriopheophytins (BPhes). This protein presents unique opportunities for studying biological electron transfer, as Zn-containing chlorins can exist in 4-, 5-, and (theoretically) 6-coordinate states within the RC. In this paper, the electron transfer perturbations attributed exclusively to coordination state effects are separated from those attributed to the presence, absence, or type of metal in the bacteriochlorin at the H_A pocket of the RC. The presence of a 4-coordinate Zn^{2+} ion in the H_A bacteriochlorin instead of BPhe results in a small decrease in the rates of the $P^* \rightarrow P^+H_A^- \rightarrow P^+Q_A^-$ electron transfer, and the charge separation yield is not greatly perturbed; however coordination of the Zn^{2+} by a fifth ligand provided by a histidine residue results in a larger rate decrease and yield loss. We also report the first crystal structure of a Zn-BChl-containing RC, confirming that the H_A Zn-BChl was either 4- or 5-coordinate in the two types of Zn-BChl-containing RCs studied here. Interestingly, a large degree of disorder, in combination with a relatively weak anomalous difference electron density was found in the H_B pocket. These data, in combination with spectroscopic results, indicate partial occupancy of this binding pocket. These findings provide insights into the use of BPhe as the bacteriochlorin pigment of choice at H_A in both BChl- and Zn-BChl-containing RCs found in nature.

1. Introduction

Photosynthetic organisms utilize light energy to generate ATP via photophosphorylation. In order to trap light energy, reaction center (RC) proteins convert electronic excitation energy from photon absorption into charge separation. This means of charge separation relies on a cascade of ultrafast electron transfer reactions that proceeds through a series of cofactors buried within the protein. The photosynthetic RC of the bacterium *Rhodobacter sphaeroides* is the most extensively characterized and best understood RC in terms of the mechanisms of electron transfer events that result in charge separation [1–3]. The crystal structure of this protein revealed that the cofactors are arranged into two structurally largely symmetrical branches (A and B) housed within the three polypeptide subunits, designated L, M and H [4,5]. Although the two pigment branches are structurally symmetrical, they are functionally asymmetrical because the electron transfer events occur almost exclusively along the A branch, with the B branch playing a role only in the final electron transfer step.

In the initial stages of charge separation, a dimer of bacteriochlorophyll (BChl) molecules ($P_{A,B}$) located at the symmetry axis of the two pigment branches enters an excited state as a result of direct light absorption or, more commonly, excitation energy transfer from the surrounding antenna complex LH1. This excited state (P^*) decays via a 3 ps electron transfer to a nearby BChl on the A branch in a protein pocket, termed B_A, generating a $P^+B_A^-$ state within the RC. Subsequently, the B_A^- radical anion (radical anions in the RC are subsequently referred to simply as anions) reduces a nearby bacteriopheophytin (BPhe) molecule in the H_A pocket within a single picosecond, generating a $P^+H_A^-$ state. The $P^+H_A^-$ state is relatively long-lived compared to P^* and $P^+B_A^-$, lasting~200 ps before an electron transfer reaction from the H_A^- anion to a nearby quinone, Q_A. Once the RC is poised in the $P^+Q_A^-$ state, a final electron transfer reaction reduces the quinone on the B branch, Q_B. At this point, the oxidized dimeric BChls must receive an electron from a *c*-type cytochrome in the periplasm before the RC is set for another turnover, which results

Abbreviations: *E*, *Escherichia*; *R*, *Rhodobacter*; *A*, *Acidiphilium*; RC, reaction center; BChl, bacteriochlorophyll; Zn-BChl, [Zn]-bacteriochlorophyll; BPhe, bacteriopheophytin; LDAO, lauryldimethylamine-n-oxide; EADS, evolution associated difference spectra; LH1, light harvesting 1; LH2, light harvesting 2

* Corresponding author. Tel.: +1 604 822 6896.
E-mail address: j.beatty@ubc.ca (J.T. Beatty).

0005-2728/$ – see front matter © 2013 Elsevier B.V. All rights reserved.
http://dx.doi.org/10.1016/j.bbabio.2013.11.015

in the double reduction of Q_B. These electron transfers are coupled to protonation from the cytoplasm, converting Q_B from a quinone to a quinol. The quinol leaves the RC and migrates within the membrane to the cytochrome bc_1 complex, which ultimately generates a proton gradient that powers an F_0F_1 ATP synthase [6].

Spectroscopic advances over the past few decades have allowed access to the femtosecond time domain, facilitating studies of electron transfer in the RC [7]. Such experiments have shed light on some of the factors that control the rates of electron transfer, such as cofactor composition and cofactor midpoint potential, as well as the surrounding protein environment. It is generally accepted that the driving force for efficient electron transfer from B_A to H_A is dominated by the energy difference (ΔG) between the two cofactors, resulting from their different structures (BChl vs BPhe). This is true for all type II reaction centers [8]. However, a RC assembled with Zn-BChl in place of all BChls and BPhes was shown to have nearly wild type (WT) electron transfer rates [9,10]. The electron transfer rates in this Zn-RC were surprising because of the similarity of this RC's A-branch cofactor composition to the so-called β mutant RC originally characterized by Kirmaier et al. [11]. In the β mutant RC, an engineered mutation of leucine to histidine at position 214 of the M subunit ((M) L214H) resulted in a molecule of BChl being present in the H_A pocket, and this RC exhibited a ~60% yield of charge separation compared to the WT RC within a 2 ns interval after excitation [11].

In both the Zn-RC and β mutant (Mg-BChl) RC, electrons proceed from dimeric (Zn-) BChls to a monomeric (Zn-) BChl at B_A and onward to yet another (Zn-) BChl at H_A. Apparently the H_A Zn-Bchl is not converted to BPhe because the Zn^{2+} ion is more tightly bound to the bacteriochlorin macrocycle than a Mg^{2+} [12]. Indeed, Zn-BChl is found in the RC and antenna complexes of an acidophilic photosynthetic bacterium, *Acidiphilium rubrum* [13], which lives at low pH (2.5–6) where Mg-containing BChl would potentially be converted to BPhe [13]. Lin et al. postulated that in addition to the difference of a Mg^{2+} vs. Zn^{2+} ion in the H_A bacteriochlorin, the difference in coordination state of the metal in the bacteriochlorin in the H_A pocket was responsible for a change in electron transfer rates by a factor of about two in these two RCs that contain a Zn- or Mg-BChl in place of BPhe in the H_A pocket [9].

In the case of the β mutant RC studied previously, the central Mg^{2+} in the H_A BChl was thought to be 5-coordinate [11]. In the Zn-RC, the analogous H_A cofactor was proposed to be 4-coordinate, consistent with an absorption spectrum more similar to BPhe than a 5-coordinate BChl in the Q_x transition region [9,14]. Previous work has indicated a correlation between Q_x transition energy and redox potential in metallo-bacteriochlorins, implying that the redox potential of the Zn-BChl in the H_A pocket may be close to that of BPhe [15,16].

In a hole-burning study of the Zn- and Zn-β-RC (the Zn-β-RC contains the (M) L214H mutation of the β mutant engineered in a *bchD* mutant background), it was proposed that the quantum yield of $P^+Q_A^-$ formation decreased by 40% in the Zn-β-RC, relative to the Zn-RC. This estimate was based on the assumption that the $P^+Q_A^-$ lifetime is similar in the two RCs [10]. The H_A Zn-BChl was proposed to be 5-coordinate in the Zn-β-RC, based on the presence of the (M) L214H side chain and the disappearance of a 542 nm peak (attributed to the $H_{A,B}$ Q_x transition) in low temperature absorption spectra. However, this was a larger absorbance change than expected, as it was thought that the $H_{A,B}$ Q_x transition peak should decrease by only ~50% as a result of H_A Zn-BChl pentacoordination [10]. Several explanations were offered, because there were uncertainties about whether the H_B or carotenoid cofactor was present, and whether the H_B Zn-BChl was present but as 5-coordinate (perhaps with water as the fifth Zn^{2+} ligand) [10]. Furthermore, the forward and back electron transfer rates in the pathway between P and Q_A were not addressed.

Here, the effects of coordination state of a metal-containing bacteriochlorin in the H_A pocket on RC structure and function are explored in more detail by directly comparing two RCs containing six Zn-BChls, and that differ only in whether leucine or histidine is present at M214. The Zn-BChl-containing RC with (M)214-leucine (Zn-RC) is compared to the Zn-BChl-containing RC with M214-histidine (Zn-β-RC) using absorption spectroscopy, X-ray anomalous scattering and structure analysis of protein crystals, and femtosecond transient absorption spectroscopy. For clarity, the RCs in this study are henceforth called the WT-RC, WT-β-RC (meaning the (M) L214H mutation), Zn-RC, and Zn-β-RC. Using these RCs, the effects attributed to the presence or absence of a central metal at H_A were separated from those attributed to protein ligation and hence coordination state. Our results suggest that there is a small decrease in charge separation yield due to the mere presence of a Zn^{2+} ion in the bacteriochlorin at H_A, and a larger yield loss upon formation of 5-coordinate Zn-BChl. Furthermore, we report structural differences at H_B that appear to result from the substitution of Zn-BChl for BChl. These data are discussed in the context of (i) the consequences of metal coordination vs. axial ligation at H_A, on RC function, (ii) the preference for BPhe in photosynthetic RCs, even in an organism that naturally incorporates Zn-BChl into the RC, and (iii) the general effects of alternative pigment production in photosynthetic bacteria.

2. Materials and methods

2.1. Bacterial strains, plasmids and cultures

Starter cultures of *R. sphaeroides* were grown in RCV medium aerobically in the dark [17]. These cultures were used to seed small chemotrophic RLB medium [18] cultures which were grown semi-aerobically in the dark at 150 RPM in 250 mL conical flasks. These cultures were then used to seed 5.6 L of RLB media (25 mL inocula added to 4 × 2 L conical flasks each containing 1.4 L of media), which were shaken at 150 RPM in the dark. *Escherichia* (*E.*) *coli* strain DH10B was used for cloning and site-directed mutagenesis. *R. sphaeroides* strains ΔRCLH and ΔRCLH/Δ*bchD* were previously described [10,19]. The previously described plasmids pRS1 and pRS1::(M) L214H were transferred from *E. coli* strain DH10B to *R. sphaeroides* strain ΔRCLH/Δ*bchD* by conjugation [20].

2.2. Isolation of reaction centers

His-tagged RCs were isolated from 5.6 L of culture according to the procedure of Saer et al. [20], essentially a modified version of the method of Goldsmith and Boxer [20,21]. RCs were dialyzed against 10 mM Tris, 0.025% LDAO and stored at −80C for later use. To obtain sufficient amounts of Zn-BChl-containing RCs, the cell culture volume was scaled up to 72 L because of the low yield of these RCs from *bchD* mutant strains. RCs used in protein crystallography were never frozen and subsequently purified by FPLC using a SourceQ column prior to hanging drop experiments.

2.3. Ground state absorption spectroscopy

Ground state absorption spectra of purified RCs in 10 mM Tris (pH 8.0), 0.025% LDAO mixed with an equal volume of glycerol were obtained at 10 K with an ARS helium cryostat and a Cary 6000*i* spectrophotometer using the same methods and instrumentation described by Saer et al. [20]. Where necessary, a monotonic increase in background absorbance (500 to 730 nm) resulting from light-scattering was corrected by subtracting a linear function.

2.4. Time-resolved spectroscopy

The femtosecond transient absorption spectrometer utilized was the same setup described in Pan et al. [22]. Transient absorption changes from a spectral range of 500–980 nm, and a time range of 0.5 ps before and 6 ns after the excitation pulses, were recorded. RC samples were loaded in a 9 cm diameter spinning wheel (~10 revolutions per second) with an optical path length of 1.2 mm at an optical density of ~0.8 at

800 nm. Global analysis of the datasets was performed with ASUFIT, a locally-written program created in the MATLAB environment.

2.5. X-ray crystallography

Crystals of the Zn-RC were formed using the hanging drop technique outlined in Saer et al. [20]. Diffraction data were collected at Stanford Synchrotron Light Source on beamline 7.1 using a wavelength of 1.12709 Å and processed with Mosflm and Aimless to 2.85 Å resolution [23,24]. Anomalous differences were detected to 6 Å resolution. All data sets were isomorphous with wild type RC (PDB entry 2J8C), which was used as the starting point for refinement with removal of the Mg^{2+} ions and for Zn-β-RC the side chain atoms of (M)214. Initial phases were obtained by limited refinement with Refmac5 [25] and F_o-F_c and anomalous difference maps were computed with Coot [26] and FFT, respectively. Based on the peaks observed in both maps, Zn-BChl was modeled at each of the P, B, and H cofactor sites in both the A and B branches. Density for a histidine side chain was observed at residue (M)214 in the Zn-β-RC and modeled accordingly using the program Coot. Refinement of the structures was continued with Refmac5 and the removal of solvent atoms with unrealistic B-factors.

3. Results

3.1. Low temperature absorption spectroscopy

The ground state absorption spectra of the WT-RC,WT-β-RC, Zn-RC and Zn-β-RC at 10 K are shown in Fig. 1. The spectra were normalized to the amplitude of the Q_y band of the dimeric BChls ($P_{A,B}$). Characteristic absorption differences between the WT-RC and the WT-β-RC at cryogenic temperatures have been described [27]. The important features that distinguish these two RCs are the loss of the 542 nm Q_x absorption band and diminished amplitude of the 765 nm Q_y band in the WT-β-RC. These changes are accompanied by an increase in amplitude of the 600 nm Q_x band, and the emergence of a 785 nm Q_y band. Collectively, these absorption changes indicate replacement of the H_A BPhe in the WT-β-RC with a molecule of BChl. The Q_y transition differences in absorption between the Zn-β-RC and the Zn-RC are more subtle than the differences between the WT-β-RC and the WT-RC. The $P_{A,B}$ band in the Zn-β-RC is slightly broadened relative to the Zn-RC, and the $B_{A,B}$ and $H_{A,B}$ Q_y bands of the Zn-β-RC appear to be shifted ~2 nm to the blue. In the Q_x transition region of the Zn-β-RC spectrum, several features indicate the conversion of the 4-coordinate Zn-BChl at H_A in the Zn-RC to 5-coordinate in the Zn-β-RC: the increased amplitude of the ~590 nm peak corresponding to a 5-coordinate Zn-BChl, accompanied by the disappearance of a peak at ~560 nm, where the 4-coordinate Zn-BChl absorbs in the Zn-RC [9,10]. The H_B Zn-BChl content in the Zn-RC appears to be low, because the peak at ~560 nm seems too small to represent contributions from two Zn-BChls (compare this region in the Zn-RC to the WT-RC, which shows two distinct peaks of roughly the same size).

The bandwidth of $P_{A,B}$ absorption in the Q_y transition for both the WT-β and Zn-β-RC appears slightly broadened on the shorter wavelength side relative to their non-β counterparts. Therefore, although (M)H214 should not be in the immediate vicinity of the macrocycle component of the dimeric (Zn-)BChls, it appears that this change slightly perturbs this region. The highest resolution crystal structure available for the RC shows that (M) L214 lies close to the phytyl tail of the P_A BChl [28]. Thus, it appears that this bandwidth increase may be a consequence of an interaction between the histidine residue at (M)214 and the P_A tail. Alternatively, the (M)L214H mutation may induce a small perturbation in the membrane-spanning helix (helix D) in which this residue resides. Because this helix also contains residue (M)H202, which acts as the fifth coordinate to P_B [29], changes in (M)214 may contribute to changes in $P_{A,B}$ Q_y absorbance through minor variations of the P_B-(M)H202 bond.

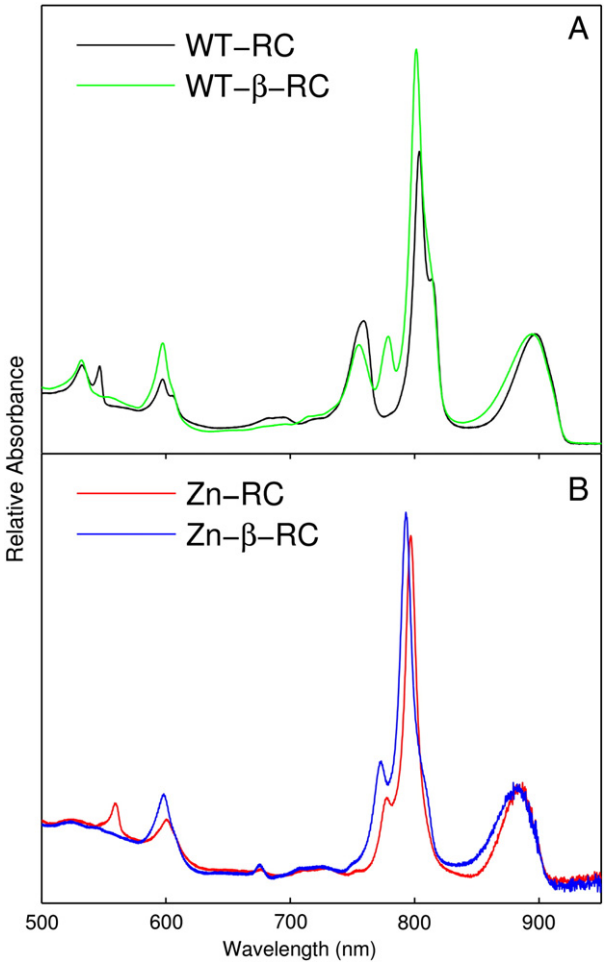

Fig. 1. Ground state absorption spectra obtained at 10 K for (A) the WT (black), and β mutant RCs (green), and (B) the Zn-RC (red) and Zn-β RCs (blue). The spectra were normalized to the P865 absorption maximum. The spectrum of the Zn-RC was corrected for scatter by subtracting a straight line from 500 to 730 nm.

3.2. X-ray crystallography and anomalous scattering

To elucidate the type, coordination state and occupancy of the bacteriochlorin cofactors in Zn-BChl-containing RCs, the crystal structures of the Zn-RC and Zn-β-RC were solved to a resolution of 2.85 Å. The refinement statistics are listed in Table 1. Overall, the structures resemble that of the native RC (PDB entry 2J8C). In both the Zn-RC and Zn-β-RC structures, the iron, carotenoid and all the bacteriochlorin cofactors are present.

An electron density map was computed from the anomalous difference data collected above the Zn-edge of the two RC structures to reveal the location of Zn^{2+} ions within the two structures (Table 2). A peak greater than 4σ was observed in the anomalous maps at the center of all bacteriochlorin-type cofactors indicative of the presence of Zn^{2+} ions at these sites. At the wavelength used for data collection, the anomalous signal from Mg^{2+} is weak and would not significantly contribute to the density observed in the map. The signal from iron can be used as an internal standard and indeed peaks at 8.7σ and 10σ were observed at the iron site in the Zn-RC and Zn-β-RC structures, respectively. In the Zn-RC structure, five of the bacteriochlorin cofactors appear to be bound at full occupancy based on refined Zn^{2+} ion B-factors of 58 $Å^2$ or less and anomalous map peaks > 12σ. In contrast, the larger B-factor of the Zn atom at H_B site (86 $Å^2$), in combination with the lower anomalous map peak (7σ) imply a lower occupancy and/or a higher degree of disorder of this cofactor. The H_B cofactor in the Zn-β-RC structure exhibits even lower occupancy and/or greater disorder (Table 2). These

Table 1
X-ray data collection and refinement statistics for Zn-RC and Zn-β-RC.

Structure		Zn-RC	Zn-β-RC
Accession code		4N7K	4N7L
Unit cell parameters	$a = b$	139.45 Å	139.59 Å
	c	184.18 Å	184.05 Å
Resolution (Å)		73.23–2.85 (2.90–2.85)	69.79–2.85 (2.90–2.85)
R_{merge}		0.105 (0.972)	0.098 (0.705)
I/σI		10.5 (1.5)	12.6 (2.4)
Multiplicity		6.2 (4.7)	7.0 (6.2)
Completeness (%)		96 (95)	87.4 (85.6)
R_{work}		0.182	0.167
R_{free}		0.242	0.216
Wilson B-factor (Å^2)		53.1	47.0
Overall B-factor (Å^2)		58.2	54.8
Coordinate error[a] (Å)		0.21	0.17
Bond length rmsd (Å)		0.011	0.013
Bond angle rmsd (°)		2.6	2.7

Numbers in parentheses reflect statistics for the highest resolution shell.
[a] Coordinate error is the estimated standard uncertainty from maximum likelihood refinement.

values for the H_B cofactor in both the Zn-RC and Zn-β-RC, relative to the values for the other bacteriochlorin cofactors, indicate that the H_B pocket is not well-occupied, and perhaps less well-occupied in the Zn-β-RC than in the Zn-RC. Such a decrease in occupancy may provide a rationale for the absence of a Q_x transition H_B peak (Fig. 1 and Neupane et al.) [10]. Interestingly, the B-factors of the amino acid residues surrounding the H_B cofactor were similar to those in the rest of the protein, indicating that the observed disorder was centered on the Zn-BChl molecule itself, and not the surrounding protein.

In comparison to the H_B site, the B_B, $P_{A/B}$, and A-branch Zn-BChls of the Zn-β-RC and Zn-RC appear to be relatively well-ordered and fully occupied, based on the anomalous signal intensity and B-factor values, which are similar to the mean values of each respective structure (Table 2). A side by side comparison of the H_A cofactors for the Zn-RC and Zn-β-RC can be seen in Fig. 2. For Zn-BChl in sites with a His residue available for coordination, the imidazole ring is observed 2.1 to 2.4 Å from the Zn^{2+} ion. At the Zn-RC H_A site (with a Leu present), the side chain is separated by 3.2 Å from the Zn^{2+} ion of the Zn-BChl. Although at 2.85 Å resolution for these structures the error estimate of these distances is ±0.3 Å, at all of the Zn-BChls the electron density maps indicate the absence of an externally-derived metal ligand, such as water. Therefore, we suggest that the major structural difference between the A-branch electron transfer carriers in the Zn-RC and Zn-β-RC is the coordination state of the Zn^{2+} ion in the H_A Zn-BChl, which is 4-coordinate in the Zn-RC and 5-coordinate in the Zn-β-RC.

3.3. Time-resolved spectroscopy

Upon RC excitation with an 860 nm pulse, P forms an excited state (P*) resulting in stimulated emission which dominates the absorbance change signal near 925 nm (Fig. 3). P* then decays by charge separation on the picosecond time scale forming the $P^+H_A^-$ state, or possibly a mix of $P^+B_A^-$ and $P^+H_A^-$, also called $P^+I_A^-$ [27]. Global analysis of the time-resolved spectra for all four RCs was performed over the Q_x wavelength region from 500 to 750 nm and Q_y region from 700 to 960 nm, by fitting to a sequential reaction model (A → B → C …). The time constants of each reaction step, in addition to the yields of charge separation and calculated ground state recombination rates, are compiled in Table 3. The fit in the Q_y region for the decay of P*, representative of forward electron transfer to the nearby B_A cofactor (and subsequently to H_A), yielded time constants of 3.8 ps for the WT-RC, 3.9 ps for the Zn-RC, 4.8 ps for the WT-β-RC, and 5.5 ps for Zn-β-RC (Table 3). Thus, initial electron transfer takes place on the picosecond time scale for all four RCs

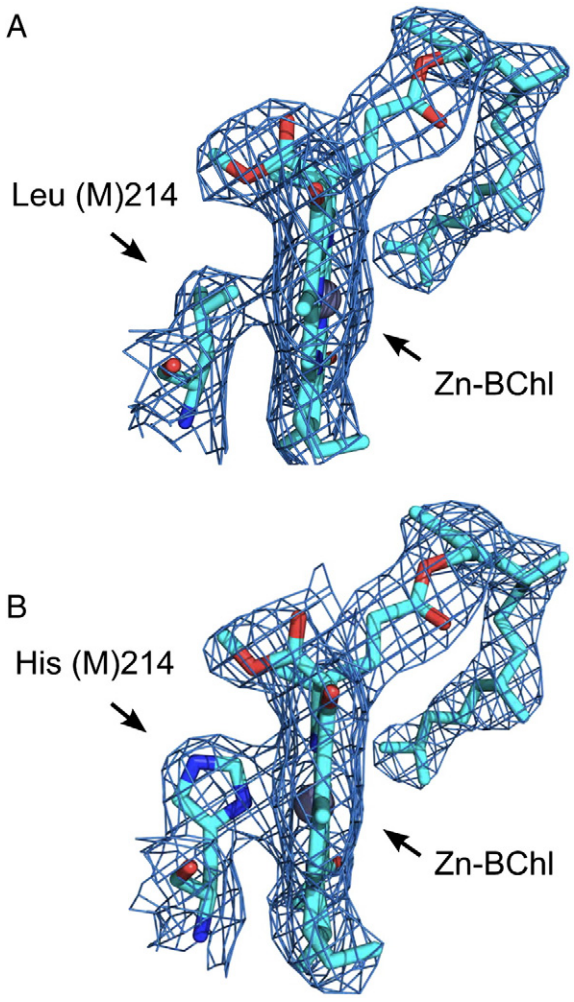

Fig. 2. Stick models and electron density (mesh) of the H_A cofactor and axial (M)214 residues from the crystal structures of the (A) Zn-RC and (B) Zn-β-RC. The distances from the axial residues to the macrocycle centers are 3.9 Å and 2.1 to 2.4 Å for the Zn-RC and Zn-β-RC, respectively. Color code: teal, carbon atoms; blue, nitrogen atoms; red, oxygen atoms.

Table 2
Anomalous map statistics for metals in the Zn-RC and Zn-β-RC X-ray diffraction datasets.

Site	Zn-RC				Zn-β RC			
	Omit*Fo-Fc* peak (σ)	Anomalous map peak (σ)	Zn B-factor (Å^2)	Leu/His-Zn distance (Å)	Omit *Fo-Fc* peak (σ)	Anomalous map peak (σ)	Zn B-factor (Å^2)	Leu/His-Zn distance (Å)
P_A	25	13	50	2.1	25	16	43	2.2
P_B	25	13	50	2.1	24	14	44	2.2
B_A	25	14	44	2.2	25	15	39	2.3
B_B	24	14	39	2.4	25	16	37	2.5
H_A	20	12	58	3.2	26	15	43	2.3
H_B	13	7	86	3.6	11	4	113	3.9
Fe	24	9	45	–	24	10	41	–

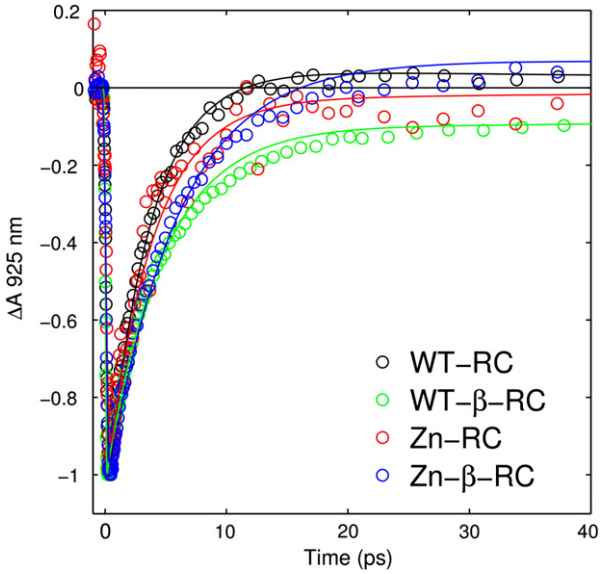

Fig. 3. Kinetic traces of stimulated emission decay for WT, β mutant, Zn-, and Zn-β RCs at 925 nm. Data points are shown as open circles, whereas the fits are shown as solid lines. The data were normalized to the maximum level of bleaching.

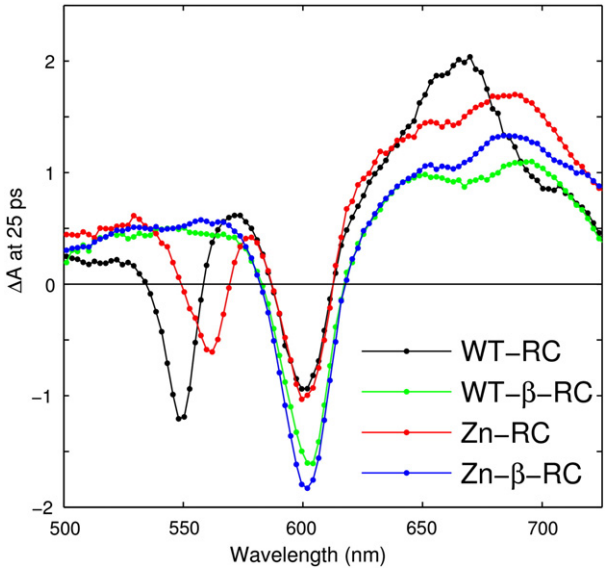

Fig. 4. Transient absorption difference spectra of the Q_x transitions of WT and mutant RCs 25 ps after excitation, representative of the $P^+I_A^-$ state. The data were normalized to the Q_x bleaching maximum of P* (~600 nm) at 0.5 ps post-excitation.

although the rates of the WT-RC and Zn-RC group together, separately from the rates of the WT-β-RC and Zn-β-RC.

Previous absorption and fluorescence studies have shown that it is possible to resolve a second decay phase from the P* kinetics for datasets in which a high signal-to-noise ratio of the data is achieved [30,31]. Our fitting revealed the presence of a second decay phase in all four RCs studied. While the amplitudes of this phase were small compared to the initial phase of P* decay (23% for the WT-RC; 31% for the WT-β-RC; 34% for the Zn-RC; and 32% for the Zn-β-RC), the presence of this component was required to obtain a good fit of the data. The lifetimes of the longer decay phase were 11 ± 5 ps for the WT-RC, 11 ± 7 ps for the Zn-RC, 18 ± 5 ps for the WT-β-RC, and 22 ± 5 for the Zn-β-RC (Table 3).

Transient absorption difference spectra from 500 to 725 nm for all RCs at 25 ps after excitation are shown in Fig. 4. The spectra were normalized to the P* bleaching maximum near 600 nm at 0.5 ps. In the Zn-RC, there is an absorption decrease near 560 nm, attributed to bleaching of the Zn-BChl in the H_A site because this wavelength corresponds to the Q_x absorption maximum of this cofactor in the ground state (Fig. 1). Like the ground state transition, the magnitude of this bleaching is substantially less than that of the corresponding H_A bleaching in the WT-RC at ~545 nm (we assume similar extinction coefficients). In contrast, the magnitude of absorbance decrease near 600 nm, which represents ground state bleaching of P on this time scale, is nearly identical in the WT-RC and Zn-RC.

In the Zn-β-RC there is no ground state absorbance in the 545 to 560 nm region (Fig. 1), and therefore no ground state bleaching in this region of the difference spectrum (Fig. 4). However the bleaching at ~600 nm is increased compared to both the WT-RC and Zn-RC. This is consistent with ground state absorption measurements of the Zn-β-RC at low temperatures, which show that the H_A Zn-BChl absorbs maximally at 598 nm, overlapping the ground state bands of P, B_A and B_B (Fig. 1) [10]. The red shift from ~545 to ~600 nm in both the ground state absorption spectrum and the difference spectrum of the WT-β-RC results from conversion of BPhe to His-coordinated BChl, whereas in the Zn-β-RC the analogous shift is consistent with a Zn-BChl coordination state change at H_A from 4- to 5-coordinate.

A prominent feature of the $P^+I_A^-$ absorption spectrum of all these RCs is the large broadband absorption increase in the ~620 to 725 nm region (Fig. 4), primarily due to anion absorption in this region. The peak of this absorbance increase shifts from ~660 nm in the WT-RC to ~680 nm in the WT-β-RC, as shown previously [27]. In both the Zn-RC and Zn-β-RC, the portion of this maximum is intermediate in wavelength between that of the WT-RC and the WT-β-RC. The fact that the two Zn-BChl-containing RCs share a $P^+I_A^-$ absorption maximum at a similar wavelength, and which differs from that of both the WT-RC and the WT-β-RC indicates that the position of the anion absorption peak is sensitive to both the presence and identity of the metal associated with the H_A bacteriochlorin, but insensitive to its coordination state.

The absorbance between ~620 and 725 nm associated with the I_A^- anion decays in the WT-RC with a time constant of 200 to 250 ps, as shown for the 675 nm wavelength in Fig. 5, in agreement with previous work [9,30,32,33]. The decay of the I_A^- anion band in the Zn-RC has a time constant of ~290 ps (Fig. 5, Table 3), as seen previously [9]. In both the WT-β-RC mutant and Zn-β RCs, much longer time constants of ~560 ps and ~640 ps, respectively, were resolved from the fitting (Table 3). Note that minima of larger uncertainty (±50 ps) were found in the fits for the WT-β-RC and Zn-β-RC compared to the WT

Table 3
Calculated transient state lifetimes, reaction rates and final yields of charge separation for RCs in this study based on global analysis.

Sample	P* (fast)	P* (slow)	$P^+I_A^-$	τ_{IQ}[a]	τ_{rec}[b]	ϕ[c] ($P^+Q_A^-$)
WT-RC	3.8 ± 0.2 ps	11 ± 5 ps	210 ± 30 ps	0.2 ns	20 ns[d]	100%
WT-β-RC	4.8 ± 0.5 ps	18 ± 5 ps	560 ± 100 ps	4.0 ± 0.7 ns	0.65 ± 0.1 ns	14%
Zn-RC	3.9 ± 0.7 ps	11 ± 7 ps	290 ± 50 ps	0.4 ± 0.1 ns	1.1 ± 0.2 ns	74%
Zn-β-RC	5.5 ± 0.2 ps	22 ± 5 ps	640 ± 90 ps	6.4 ± 0.9 ns	0.71 0.1 ns	10%

[a] Calculated rate of forward electron transfer from I_A^- to Q_A using Eq. (2).
[b] Calculated rate of recombination using Eq. (1).
[c] Calculated yield of $P^+Q_A^-$ based on the amount of P^+ bleaching amplitude (measured at 860 nm) at the end of the measurement window compared to 45 ps post excitation.
[d] Based on measurements in which Q_A was removed from the RC.

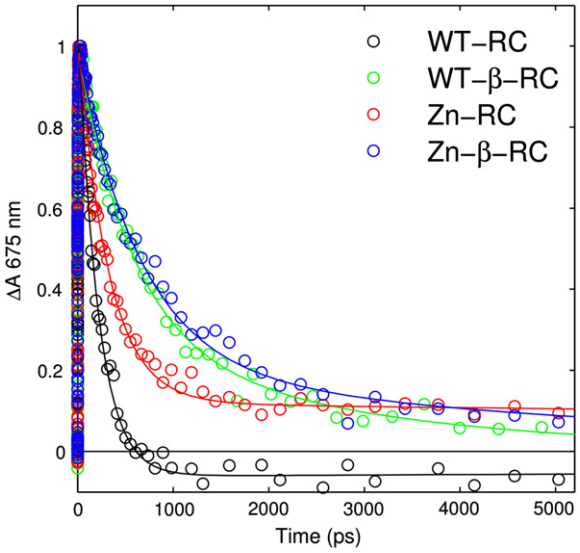

Fig. 5. Kinetics of $P^+I_A^-$ state decay at 675 nm for WT and mutant RCs measured up to 5500 ps. Spectra were normalized to the maximum amplitude increase at 675 nm. Open circles represent raw data points, and solid lines are representative of fits to the data.

and Zn-RCs. The analysis of this complication will be given in the Discussion section.

In Fig. 6, the fitting results for each type of RC are represented as evolution-associated difference spectra (EADS) [34]. This representation allows simplified visualization of the spectral progression associated with the decay times of the fit, and is not meant to depict the spectra of the actual excited and charge separated state populations (which would require the application of a specific kinetic model). As can be seen, the values of the time constants for the hundreds of picoseconds EADS for the WT-RC and Zn-RC (210 ps and 290 ps, respectively) are more similar to each other than to the time constants found for the WT-β-RC and the Zn-β-RC (560 ps and 640 ps, respectively). Furthermore, the EADS with the longest time constant in both the WT-RC and Zn-RC was non-decaying (*i.e.*, greater than 3 times the time window of measurement), whereas the WT-β-RC and the Zn-β-RC did not contain such a long-lived component. Thus, the kinetic behavior of the 4-coordinate Zn-BChl at H_A is more like that of a BPhe than a 5-coordinate (Zn-)BChl. All of the mutants, including the Zn-RC, however, appear to have lower $P^+Q_A^-$ yields than the WT-RC on the nanosecond time scale. This can be seen in Fig. 6 by comparing the bleaching of P near 860 nm in the green EADS component that has a lifetime of hundreds of picoseconds, with that of the red (nanosecond, or non-decaying) component. In the WT-RC, there is no significant decrease in the amplitude of the bleaching signal over this time, as would be expected for 100% yield of charge separation. In contrast, each of the mutants shows a partial decrease in bleaching amplitude. In the case of the Zn-RC, this decrease is relatively small (74% of the bleaching amplitude remains; Table 3), however this amplitude is still much larger than those of the WT-β-RC and the Zn-β-RC (14% and 10%, respectively; Table 3). In our experiments, the degree of P^+ remaining in the WT-β-RC at the end of the measurement, as indicated by the difference in bleaching amplitude at 70 nm between 45 ps post excitation and the end of the measurement window, was less than reported previously by Kirmaier et al. because our experiments used a longer measurement window (5.5 ns vs. 2.7 ns), which revealed additional amounts of ground state recombination [32]. Note that there is no evidence for any yield loss on the picosecond time scale in either the WT or mutant RCs. This can be seen by the invariance between the blue (few picoseconds) and green (hundreds of picoseconds) EADS near 830 nm in Fig. 6.

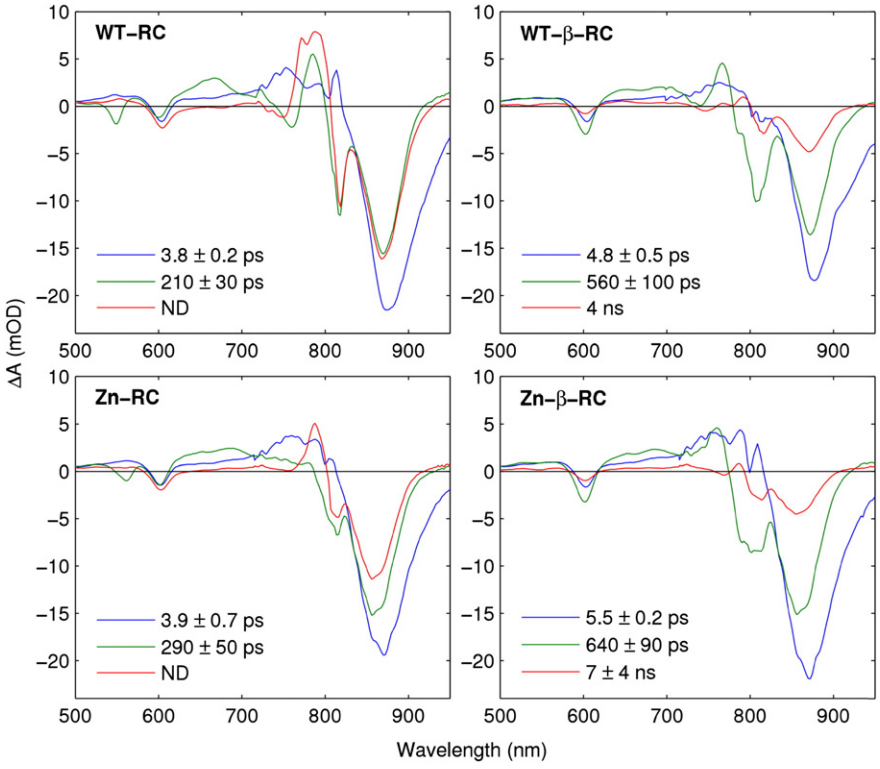

Fig. 6. Evolution associated difference spectra (EADS) of the Q_x and Q_y transitions of the RCs measured in this study. The solid black line is a zero absorbance reference line. Each RC was fit to a fast < 10 ps component, a hundreds of ps component, and a nanosecond or non-decaying component. Component lifetimes are representative of best fits to the transient absorption spectrum datasets using a least squares fitting approach. Deviations represent the overlap of 5% variations in the χ^2 (goodness of fit) values between independent fittings of the Q_x and Q_y datasets.

At this wavelength, there is essentially no contribution in the picosecond spectrum from stimulated emission, and so one can monitor the decay of ground state bleaching independently.

4. Discussion

4.1. Functional analysis of Zn- and Zn-β RCs

We have exploited the Zn-BChl-containing RCs to evaluate the effects of changing the H_A cofactor coordination state on electron transfer in the RC. This comparison would be impossible in the (Mg^{2+}-) BChl-containing RC because the H_A pocket contains BPhe when a fifth ligand is absent [20]. Evidently the Zn^{2+} ion is more tightly bound to the bacteriochlorin macrocycle than Mg^{2+}, and so Zn-BChl is resistant to whatever mechanism is responsible for the dechelation of BChl to yield BPhe [12,20,35].

The kinetic consequences of substituting Zn-BChl into the RC in an otherwise WT background were previously studied, and it was found that the Zn-RC functions similarly to the WT RC [9]. However, our EADS data now indicate a slower rate of electron transfer from H_A to Q_A for the Zn-RC. The EADS with a hundreds of ps time constant for the Zn-RC fitted best to ~290 ps, compared to ~210 ps in the WT RC. The difference between our experimental values and those previously obtained by Lin et al. likely stems from our use of a broadband detection setup, in contrast to a single wavelength detector [9]. Furthermore, the final charge separation yields of the Zn-RC were also lower, with evidence of some $P^+I_A^-$ recombination in the non-decaying EADS. In this respect, the Zn-RC is more similar to the WT-β-RC and Zn-β-RC because the presence of ground state recombination on this time scale suggests the rate of recombination from $P^+I_A^-$ is increased. The rate of recombination in the Zn-RC was thus calculated based on the observed lifetime of the $P^+I_A^-$ state and the amount of P^+ remaining at the end of the time window of the experiment according to the formula:

$$\tau_{rec} = \tau_{obs}/((100–\phi)/100) \quad (1)$$

where τ_{rec} is the rate of recombination, τ_{obs} is the $P^+I_A^-$ lifetime, and ϕ is the final yield of P^+ [32]. For the Zn-RC, this yielded a value of 1.1 ns, a value closer to that of the WT-β-RC and Zn-β-RC (651 ps and 711 ps, respectively) than the 20 ns value obtained for the WT-RC from which Q_A had been removed (Table 3) [36].

The relatively long-lived hundreds of ps EADS obtained for the WT-β-RC from our datasets compared to previously published $P^+I_A^-$ lifetimes suggests a degree of heterogeneity in the $P^+I_A^-$ decay [32,37]. When our datasets were truncated to a shorter time window (2 ns), the $P^+H_A^-$ decay rates were found to be closer to the previously reported rates (data not shown). The slower rates observed in the WT-β-RC and the Zn-β-RC likely reflect more complex kinetic heterogeneity than can be described by four exponential components, reflecting an average of forward electron transfer as well as ground state recombination from RCs in the $P^+I_A^-$ state. A previous analysis of the kinetics of the WT-β-RC in which electron transfer to Q_A was blocked demonstrated that the recombination rate from P^+I^- was approximately 1 ns (compared to~20 ns in the WT-RC) [32]. Furthermore, our calculated charge recombination rates in the WT-β-RC, and Zn-β-RC suggest that charge recombination occurs much faster than in the WT-RC. This difference likely contributes to the relatively shallow fitting minima obtained in the WT-β-RC and Zn-β-RC for this EADS (compare the deviations between the WT-RC/Zn-RC and WT-β-RC/Zn-β-RC in the green spectra of Fig. 6). Because the Zn-RC also has a more rapid rate of charge recombination relative to the WT-RC, we suggest that the presence of the metal center at H_A in the Zn-RC results in an H_A^- anion that is closer in energy to B_A^- compared to the WT-RC, as previous mutagenic studies on RCs have found a strong correlation between the rate of $P^+H_A^-$ recombination and the similarity of B_A^- and H_A^- energies [38]. Clearly, this energetic proximity of H_A^- to B_A^- is lesser in the Zn-RC compared to the WT-β-RC and Zn-β-RC, because the $P^+H_A^-$ recombination rate of the Zn-RC is relatively slow.

In addition to the rate of recombination, it was also possible to extract information on the rates of forward electron transfer from I_A^- to Q_A, by taking into account the lifetime of the hundreds of ps EADS, as well as the final $P^+Q_A^-$ yield of each RC. The rate of electron transfer was calculated according to the equation:

$$\tau_{QT} = \tau_{obs}/(\phi/100) \quad (2)$$

where τ_{QT} is the rate of electron transfer, τ_{obs} is the $P^+I_A^-$ lifetime, and ϕ is the final yield of P^+ [32]. The values of τ_{QT} are 0.2 ns for the WT-RC, 4 ns (WT-β-RC), 0.4 ns (Zn-RC), and 6.4 ns (Zn-β-RC). From these data, it appears that the presence of a fifth coordinate at the H_A metal center is associated with a much reduced rate of forward electron transfer from I_A^- to Q_A.

The greater similarity of Zn-RC kinetic behavior to that of the WT-RC, than to the WT-β-RC and Zn-β-RC, evidently is because the H_A cofactor is a 4-coordinate Zn-BChl. This indicates that the five-coordinate center present in the latter two RCs is the key player in the observed low yields of charge separation, and that the presence or absence of a metal in the H_A bacteriochlorin is of less consequence. One explanation for the observed results stems from the Q_x transition energies of the H_A cofactors among these RCs. Previous studies on metal-substituted bacteriochlorins *in vitro* have reported a linear correlation between Q_x transition energies, redox potential, and electronegativity (Pauling values) of the bacteriochlorin metal center [15,16]. We suggest that the 4-coordinate Zn-BChl at H_A functions similarly to a BPhe molecule because the Zn-BChl transition energy, redox potential, and central ion electronegativity are closer to that of BPhe (as indicated by the Q_x aborption peak) than a 5-coordinate BChl or Zn-BChl. In the case of central ion electronegativity, although the Pauling value for Zn^{2+} (~1.6) is closer to Mg^{2+} (~1.3) than H (~2), this value is similar to both and lies between Mg^{2+} and H. Additionally, an increase in the coordination state of the metal center of a bacteriochlorin has been associated with a lower electronegativity value for the metal [16]. Thus, a 5-coordinate Zn-BChl should be less electronegative than both the 4-coordinate counterpart and BPhe.

In addition to the observed kinetic differences upon entering the $P^+I_A^-$ state, the presence of a metal at H_A imbues different spectroscopic properties on the I_A^- anion. The transient absorption spectra of the $P^+I_A^-$ state for Zn-BChl-containing RCs are more similar to each other (and the WT-β-RC) than the WT-RC in the 650–730 nm region. As noted in the Results section, the WT-RC has an absorption maximum at higher energy in this region compared to the other 3 RCs. Thus, the red-shifted peak in these three RCs appears to be a correlated with the presence of a metal at H_A, regardless of coordination state or the type of metal present.

Interestingly, the RC of the photosynthetic bacterium *A. rubrum* contains Zn-BChl in place of BChl, but this organism contains BPhe at H_A. In this organism, Zn-BChl is presumably synthesized by Mg-containing BChl synthesis intermediates [39]. After the final step of BChl synthesis, it is thought that the low environmental pH promotes pheophytinization BChl, at which point a Zn^{2+} atom incorporates into the chlorin macrocycle by an unknown mechanism [39]. This theoretically provides a pool of both Zn-BChl and BPhe with which the apo-RC can selectively incorporate. This mechanism of Zn-BChl biosynthesis is different from that of the *R. sphaeroides bchD* mutant, because this mutant utilizes Zn-containing synthesis intermediates. Although electron transfer has been studied only to the $P^+H_A^-$ state in *A. rubrum* [40], we speculate that in this RC the rate of electron transfer to Q_A is like that in the WT-RC. Based on our results, it appears that natural selection would favor the presence of BPhe at H_A in evolution because it results in a much slower decay of $P^+I_A^-$ via charge recombination.

4.2. Consequences of the absence of Mg-BChl

In the ground state absorption spectra of the Zn-RC, as well as in previous low temperature measurements, a single peak was present in the Q_x region near 560 nm, originally attributed to overlapping absorption of 4-coordinate Zn-BChls in the $H_{A,B}$ pockets [9,10]. However, as reported by Neupane et al. and confirmed here, the Zn-β-RC has little or no absorption around 560 nm, whereas it would be thought that only the component due to the H_A Zn-BChl would be shifted as a result of the (M) L214H mutation, as is seen when this mutation is introduced into the WT RC (Fig. 1) [10]. Neupane et al. offered three possible explanations for the absence of a defined H_B peak in the Q_x region of the Zn-β RC [10]. Our crystal structures show that, relative to the WT-RC, the Zn-BChl in the H_B pocket of the Zn-RC is bound at less than full occupancy or is highly disordered, and perhaps the occupancy is even lower or disorder greater in the Zn-β-RC (Table 2). These conclusions are based on weaker density in omit difference maps of the H_B Zn-BChl, the large B-factors associated with the Zn^{2+} in the H_B pocket, and the low anomalous signal intensities for that Zn^{2+} atom (compare the values for H_B to those of the other cofactors in Table 2). Interestingly, the average B-factor of the H_B BPhe from the highest resolution RC structure currently available in the PDB database is greater than all of the other cofactors, perhaps indicating weaker binding to this pocket in the WT RC as well. As mentioned in the Results section, the B-factor for the protein component surrounding the H_B Zn-BChl is comparable to the average of the structure, consistent with the idea that the RC is a relatively rigid protein, and does not rearrange its folding due to changes in cofactor composition or even when a cavity is created by the lack of a cofactor, as was observed in pigment exclusion experiments on the H_B BPhe [41,42]. The larger Q_x spectral bandwidth of the H_B cofactor compared to H_A in is also supportive of a greater H_B site heterogeneity (Fig. 1). Additional evidence for relatively weak binding of BPhe in the WT RC H_B pocket comes from experiments involving substitution of BPhe with plant pheophytin (as well as a variety of other pigments). These experiments demonstrated that substitution is preferential in the H_B over the H_A site, consistent with a weaker binding of BPhe in the H_B pocket [43,44]. In vitro, the binding pockets for $H_{A,B}$ are selective for pheophytins, as incubation of RCs in a molar excess of metal-containing bacteriochlorins (the standard procedure for pigment exchange) resulted in substitution of pigments at the $B_{A,B}$ binding pockets instead of $H_{A,B}$ [41,45,46], The greater hydrophobicity of BPhe over BChl and Zn-BChl, as indicated by the longer retention time for BPhe in reversed-phase HPLC using a C18 column [35], may be part of the reason why binding of metal-containing bacteriochlorins to the $H_{A,B}$ pockets is weak, although it is not clear why the H_B Zn-BChl may be lost more readily or less efficiently inserted into the RC than the H_A Zn-BChl. Alternatively, it is possible that the Zn-RCs contain partially occupied H_B sites due to a lack of a sufficient quantity of available Zn-BChls in the cell. One important consequence of the *bchD* mutation yielding Zn-BChl-producing strains of *R. sphaeroides* is the severely impaired ability to synthesize the pigment [35,47]. Therefore the inability of the organism to grow photoheterotrophically is evidently because of a paucity in the cellular content of light-harvesting and RC complexes [31].

Unlike the H_B cofactors of the Zn-RC and Zn-β-RC, the H_A cofactors appear less disordered, suggesting there is no issue with the occupancy of the pocket. From a structural perspective, the H_A cofactors appear to assume a similar configuration in the two Zn-BChl-containing RCs (Fig. 2), with a possible macrocycle displacement of 0.6 Å between the two RCs. We are hesitant to make a firm conclusion on this geometric displacement between the cofactors because of the poor resolution of the data obtained for these two RCs; however the small degree of displacement is consistent with the interpretation that the differences in the functional characteristics of the two Zn-BChl-containing RCs stem from changes in H_A cofactor coordination state.

4.3. Biological implications of unnatural cofactor incorporation

Our time-resolved data demonstrate that in all 4 of these RCs $P^+I_A^-$ is achieved rapidly (within a few ps), and that differences between RCs become apparent after this state is attained. Decay kinetics of the $P^+H_A^-$ transient at 675 nm indicate that this state is relatively long-lived in the Zn-β-RC, as well as in the WT-β-RC, in agreement with previous results [11,27,32]. Furthermore, our global analysis suggests a similar degree of special pair charge recombination associated with this long-lived $P^+H_A^-$ state in the Zn-β-RC, much like in the WT-β-RC. The charge separation yields are consistent with this interpretation (*i.e.*, the WT-β-RC and the Zn-β-RC yields were 14% and 10% $P^+Q_A^-$, respectively, whereas the WT-RC and Zn-RC yields were 100% and 74% $P^+Q_A^-$, respectively). These results suggest that RCs have a degree of functional tolerance for different cofactors, and that the protein component is a key instrument in the design of an efficient charge separation pathway. The Zn-RC studied here is a case in point, as it contains a cofactor arrangement supportive of a faster rate of ground state recombination from the $P^+I_A^-$ state, but is nevertheless capable of attaining a relatively high efficiency of charge separation. This is likely because the protein scaffold of the Zn-RC has remained unchanged from its WT-RC counterpart, granting this RC the same favorable cofactor geometries and tunneling pathways available to the WT-RC. From an evolutionary perspective, this could be advantageous to photosynthetic organisms during periods of environmental change, such as a change in the wavelengths of light available, for it would allow for the continued utilization of existing protein machinery when the production of a new type of (bacterio)chlorin would provide a selective advantage. In such a case, the new pigment could be incorporated into a protein "template" with suitable geometries, which would grant the organism some degree of charge separation capability, enabling photosynthetic growth. Mutations in protein side chains may later provide further energetic optimization, resulting in a high-efficiency RC that assembles with a new pigment. For this to happen, however, the photosynthetic organism must be able to survive for some time with an inefficient RC to allow beneficial mutations to accumulate. Previous results show that LH2-lacking *R. sphaeroides* strains containing RCs with small-nonpolar side chains at H_A retain their ability to grow at low photon fluxes [20], despite the relatively low efficiencies of these RCs (compared to the WT-RC) [22], indicating that purple photoheterotrophs are indeed quite capable of surviving with lower efficiency RCs.

5. Concluding remarks

The ability to study 4- and 5-coordinate metal-containing pigments at H_A provides insights into the use of (B)Phes *vs.* (B)Chls as the pigment of choice at this position in type II RCs. Firstly, the coordination state of the central metal of BChl studied here, and perhaps other metal-chelating tetrapyrroles, affects the electron transfer properties. This effect may be due to a decrease in energy and redox potential resulting from an increase in coordination number, as observed in protein-free BChls [15,16]. Secondly, the presence of a metal in the bacteriochlorin ring, irrespective of coordination state, appears to give rise to a longer lived $P^+H_A^-$ state, however this change is minor in comparison to the introduction of a -coordinate center. Thirdly, the presence of a metal at H_A is associated with a faster rate of recombination to the ground state in the nanosecond time domain.

Acknowledgements

This work was funded by NSF grants MCB-0642260 and MCB-1157788 at ASU. JTB and MEPM thank NSERC Canada for funding through the Discovery Grants system; RGS thanks NSERC for a postgraduate fellowship; AH thanks CIHR for a Canadian Graduate Fellowship. We thank Anson Chan for preparing Fig. 2. The spectrophotometer and cryostat were funded by a Canada Foundation for Innovation

Grant to AGM. Portions of this research were carried out at the Stanford Synchrotron Radiation Lightsource, a Directorate of SLAC National Accelerator Laboratory and an Office of Science User Facility operated for the U.S. Department of Energy Office of Science by Stanford University. The SSRL Structural Molecular Biology Program is supported by the DOE Office of Biological and Environmental Research, and by the National Institutes of Health, National Institute of General Medical Sciences (including P41GM103393) and the National Center for Research Resources (P41RR001209). The contents of this publication are solely the responsibility of the authors and do not necessarily represent the official views of NIGMS, NCRR or NIH.

References

[1] A.J. Hoff, J. Deisenhofer, Photophysics of photosynthesis. Structure and spectroscopy of reaction centers of purple bacteria, Phys. Rep. 287 (1997) 1–247.
[2] R.J. Cogdell, Photosynthetic reaction centers, Annu. Rev. Plant Phys. 34 (1983) 21–45.
[3] W.W. Parson, A. Warshel, Mechanism of charge separation in purple bacterial reaction centers, in: C.N. Hunter, F. Daldal, M. Thurnauer, J.T. Beatty (Eds.), The Purple Phototrophic Bacteria, Springer, Netherlands, 2008, pp. 355–377.
[4] J.P. Allen, G. Feher, T.O. Yeates, H. Komiya, D.C. Rees, Structure of the reaction center from *Rhodobacter sphaeroides* R-26: the protein subunits, Proc. Natl. Acad. Sci. U. S. A. 84 (1987) 6162–6166.
[5] J.P. Allen, G. Feher, T.O. Yeates, H. Komiya, D.C. Rees, Structure of the reaction center from *Rhodobacter sphaeroides* R-26: the cofactors, Proc. Natl. Acad. Sci. U. S. A. 84 (1987) 5730–5734.
[6] B. Fenioux, W. Junge, Proton translocation and ATP synthesis by the FoF1-ATPase of purple bacteria, in: C.N. Hunter, F. Daldal, M. Thurnauer, J.T. Beatty (Eds.), The Purple Phototrophic Bacteria, Springer, Netherlands, 2008, pp. 475–493.
[7] R. Berera, R. van Grondelle, J.T. Kennis, Ultrafast transient absorption spectroscopy: principles and application to photosynthetic systems, Photosynth. Res. 101 (2009) 105–118.
[8] C.C. Moser, J.M. Keske, K. Warncke, R.S. Farid, P.L. Dutton, Nature of biological electron transfer, Nature 355 (1992) 796–802.
[9] S. Lin, P.R. Jaschke, H. Wang, M. Paddock, A. Tufts, J.P. Allen, F.I. Rosell, A.G. Mauk, N.W. Woodbury, J.T. Beatty, Electron transfer in the *Rhodobacter sphaeroides* reaction center assembled with zinc bacteriochlorophyll, Proc. Natl. Acad. Sci. U. S. A. 106 (2009) 8537–8542.
[10] B. Neupane, P. Jaschke, R. Saer, J.T. Beatty, M. Reppert, R. Jankowiak, Electron transfer in *Rhodobacter sphaeroides* reaction centers containing Zn-bacteriochlorophylls: a hole-burning study, J. Phys. Chem. B 116 (2012) 3457–3466.
[11] C. Kirmaier, D. Gaul, R. DeBey, D. Holten, C.C. Schenck, Charge separation in a reaction center incorporating bacteriochlorophyll for photoactive bacteriopheophytin, Science 251 (1991) 922–927.
[12] M. Kobayashi, M. Yamamura, M. Akiyama, H. Kise, K. Inoue, M. Hara, N. Wakao, K. Yahara, T. Watanabe, Acid resistance of Zn-bacteriochlorophyll a from an acidophilic bacteria *Acidiphilium rubrum*, Anal. Sci. 14 (1998) 1149–1152.
[13] N. Wakao, N. Yokoi, N. Isoyama, A. Hiraishi, K. Shimada, M. Kobayashi, H. Kise, M. Iwaki, S. Itoh, S. Takaichi, Y. Sakurai, Discovery of natural photosynthesis using Zn-containing bacteriochlorophyll in an aerobic bacterium *Acidiphilium rubrum*, Plant Cell Physiol. 37 (1996) 889–893.
[14] T.A. Evans, J.J. Katz, Evidence for 5- and 6-coordinated magnesium in bacteriochlorophyll *a* from visible absorption spectroscopy, Biochim. Biophys. Acta 396 (1975) 414–426.
[15] D. Noy, L. Fiedor, G. Hartwich, H. Scheer, A. Scherz, Metal-substituted bacteriochlorophylls. 2. Changes in redox potentials and electronic transition energies are dominated by intramolecular electrostatic interactions, J. Am. Chem. Soc. 120 (1998) 3684–3693.
[16] G. Hartwich, L. Fiedor, I. Simonin, E. Cmiel, W. Schafer, D. Noy, A. Scherz, H. Scheer, Metal-substituted bacteriochlorophylls. 1. Preparation and influence of metal and coordination on spectra, J. Am. Chem. Soc. 120 (1998) 3675–3683.
[17] J.T. Beatty, H. Gest, Generation of succinyl coenzyme-A in photosynthetic bacteria, Arch. Microbiol. 129 (1981) 335–340.
[18] D. Jun, R.G. Saer, J.D. Madden, J.T. Beatty, Use of new strains of *Rhodobacter sphaeroides* and a modified simple culture medium to increase yield and facilitate purification of the reaction centre, Photosynth. Res. (2013) 1–9.
[19] A. Tehrani, J.T. Beatty, Effects of precise deletions in *Rhodobacter sphaeroides* reaction center genes on steady-state levels of reaction center proteins: a revised model for reaction center assembly, Photosynth. Res. 79 (2004) 101–108.
[20] R.G. Saer, A. Hardjasa, F.I. Rosell, A.G. Mauk, M.E. Murphy, J.T. Beatty, Role of *Rhodobacter sphaeroides* photosynthetic reaction center residue M214 in the composition, absorbance properties, and conformations of H(A) and B(A) cofactors, Biochemistry 52 (2013) 2206–2217.
[21] J.O. Goldsmith, S.G. Boxer, Rapid isolation of bacterial photosynthetic reaction centers with an engineered poly-histidine tag, Biochim. Biophys. Acta-Bioenergetics 1276 (1996) 171–175.
[22] J. Pan, R.G. Saer, S. Lin, Z. Guo, J.T. Beatty, N.W. Woodbury, The protein environment of the bacteriopheophytin anion modulates charge separation and charge recombination in bacterial reaction centers, J. Phys. Chem. B 117 (2013) 7179–7189.
[23] A.G.W. Leslie, H.R. Powell, Processing diffraction data with MOSFLM, Nato. Sci. Ser. II Math. (2007) 41–51.
[24] M.D. Winn, C.C. Ballard, K.D. Cowtan, E.J. Dodson, P. Emsley, P.R. Evans, R.M. Keegan, E.B. Krissinel, A.G. Leslie, A. McCoy, S.J. McNicholas, G.N. Murshudov, N.S. Pannu, E.A. Potterton, H.R. Powell, R.J. Read, A. Vagin, K.S. Wilson, Overview of the CCP4 suite and current developments, Acta Crystallogr. D Biol. Crystallogr. 67 (2011) 235–242.
[25] A.A. Vagin, R.A. Steiner, A.A. Lebedev, L. Potterton, S. McNicholas, F. Long, G.N. Murshudov, REFMAC5 dictionary: organization of prior chemical knowledge and guidelines for its use, Acta Crystallogr. D Biol. Crystallogr. 60 (2004) 2184–2195.
[26] P. Emsley, K. Cowtan, Coot: model-building tools for molecular graphics, Acta Crystallogr. D Biol. Crystallogr. 60 (2004) 2126–2132.
[27] C. Kirmaier, L. Laporte, C.C. Schenck, D. Holten, The nature and dynamics of the charge-separated Intermediate in reaction centers in which bacteriochlorophyll replaces the photoactive bacteriopheophytin.1. Spectral characterization of the transient state, J. Phys. Chem. 99 (1995) 8903–8909.
[28] J. Koepke, E.M. Krammer, A.R. Klingen, P. Sebban, G.M. Ullmann, G. Fritzsch, pH modulates the quinone position in the photosynthetic reaction center from *Rhodobacter sphaeroides* in the neutral and charge separated states, J. Mol. Biol. 371 (2007) 396–409.
[29] T.O. Yeates, H. Komiya, A. Chirino, D.C. Rees, J.P. Allen, G. Feher, Structure of the reaction center from *Rhodobacter-sphaeroides* R-26 and 2.4.1-protein-cofactor (bacteriochlorophyll, bacteriopheophytin, and carotenoid) interactions.4. Proc. Natl. Acad. Sci. U. S. A. 85 (1988) 7993–7997.
[30] S. Lin, A.K.W. Taguchi, N.W. Woodbury, Excitation wavelength dependence of energy transfer and charge separation in reaction centers from *Rhodobacter sphaeroides*: evidence for adiabatic electron transfer, J. Phys. Chem. 100 (1996) 17067–17078.
[31] M.G. Muller, K. Griebenow, A.R. Holzwarth, Primary processes in isolated bacterial reaction centers from *Rhodobacter sphaeroides* studied by picosecond fluorescence kinetics, Chem. Phys. Lett. 199 (1992) 465–469.
[32] C. Kirmaier, L. Laporte, C.C. Schenck, D. Holten, The nature and dynamics of the charge-separated intermediate in reaction centers in which bacteriochlorophyll replaces the photoactive bacteriopheophytin.2. The rates and yields of charge separation and recombination, J. Phys. Chem. 99 (1995) 8910–8917.
[33] J.L. Martin, J. Breton, A.J. Hoff, A. Migus, A. Antonetti, Femtosecond spectroscopy of electron transfer in the reaction center of the photosynthetic bacterium *Rhodopseudomonas sphaeroides* R-26: Direct electron transfer from the dimeric bacteriochlorophyll primary donor to the bacteriopheophytin acceptor with a time constant of 2.8 +/− 0.2 psec, Proc. Natl. Acad. Sci. U. S. A. 83 (1986) 957–961.
[34] I.H. van Stokkum, D.S. Larsen, R. van Grondelle, Global and target analysis of time-resolved spectra, Biochim. Biophys. Acta 1657 (2004) 82–104.
[35] P.R. Jaschke, J.T. Beatty, The photosystem of *Rhodobacter sphaeroides* assembles with zinc bacteriochlorophyll in a bchD (magnesium chelatase) mutant, Biochemistry 46 (2007) 12491–12500.
[36] W.W. Parson, R.K. Clayton, R.J. Cogdell, Excited-states of photosynthetic reaction centers at low redox potentials, Biochim. Biophys. Acta 387 (1975) 265–278.
[37] N.P. Pawlowicz, I.H. van Stokkum, J. Breton, R. van Grondelle, M.R. Jones, Identification of the intermediate charge-separated state $P^+\beta_L^-$ in a leucine M214 to histidine mutant of the *Rhodobacter sphaeroides* reaction center using femtosecond midinfrared spectroscopy, Biophys. J. 96 (2009) 4956–4965.
[38] H.Y. Wang, Y.W. Hao, Y. Jiang, S. Lin, N.W. Woodbury, Role of protein dynamics in guiding electron-transfer pathways in reaction centers from *Rhodobacter sphaeroides*, J. Phys. Chem. B 116 (2012) 711–717.
[39] T. Masuda, K. Inoue, M. Masuda, M. Nagayama, A. Tamaki, H. Ohta, H. Shimada, K. Takamiya, Magnesium insertion by magnesium chelatase in the biosynthesis of zinc bacteriochlorophyll *a* in an aerobic acidophilic bacterium *Acidiphilium rubrum*, J. Biol. Chem. 274 (1999) 33594–33600.
[40] T. Tomi, Y. Shibata, Y. Ikeda, S. Taniguchi, C. Haik, N. Mataga, K. Shimada, S. Itoh, Energy and electron transfer in the photosynthetic reaction center complex of *Acidiphilium rubrum* containing Zn-bacteriochlorophyll a studied by femtosecond up-conversion spectroscopy, Biochim. Biophys. Acta 1767 (2007) 22–30.
[41] M.R. Jones, Structural plasticity of reaction centers from purple bacteria, in: C.N. Hunter, F. Daldal, M. Thurnauer, J.T. Beatty (Eds.), The Purple Phototrophic Bacteria, Springer, Netherlands, 2008, pp. 295–321.
[42] A.J. Watson, P.K. Fyfe, D. Frolov, M.C. Wakeham, E. Nabedryk, R. van Grondelle, J. Breton, M.R. Jones, Replacement or exclusion of the B-branch bacteriopheophytin in the purple bacterial reaction centre: the H_B cofactor is not required for assembly or core function of the *Rhodobacter sphaeroides* complex, Biochim. Biophys. Acta 1710 (2005) 34–46.
[43] M. Meyer, H. Scheer, Reaction centers of Rhodobacter sphaeroides R26 containing C-3 acetyl and vinyl (bacterio)pheophytins at sites $H_{A,\ B}$, Photosynth. Res. 44 (1995) 55–65.
[44] E.M. Franken, A.Y. Shkuropatov, C. Francke, S. Neerken, P. Gast, V.A. Shuvalov, A.J. Hoff, T.J. Aartsma, Reaction centers of *Rhodobacter sphaeroides* R-26 with selective replacement of bacteriopheophytin by pheophytin *a*: I. Characterisation of steady-state absorbance and circular dichroism, and of the $P^+Q_A^-$ state, Biochim. Biophys. Acta Bioenerg. 1319 (1997) 242–250.
[45] A. Struck, H. Scheer, Modified reaction centers from *Rhodobacter sphaeroides* R26 — exchange of monomeric bacteriochlorophyll with 13^2-hydroxy-bacteriochlorophyll, FEBS Lett. 261 (1990) 385–388.
[46] H. Scheer, G. Hartwich, Bacterial reaction centers with modified tetrapyrrole chromophores, in: R. Blankenship, M. Madigan, C. Bauer (Eds.), Anoxygenic Photosynthetic Bacteria, Springer, Netherlands, 1995, pp. 649–663.
[47] P.R. Jaschke, A. Hardjasa, E.L. Digby, C.N. Hunter, J.T. Beatty, A *bchD* (magnesium chelatase) mutant of *Rhodobacter sphaeroides* synthesizes zinc-bacteriochlorophyll through novel zinc-containing intermediates, J. Biol. Chem. 286 (2011) 20313–20322.